Supplement of Atmos. Chem. Phys., 25, 4655–4664, 2025
https://doi.org/10.5194/acp-25-4655-2025-supplement

Atmospheric Chemistry and Physics
Open Access
EGU

Supplement of

Gas-phase observations of accretion products from stabilized Criegee intermediates in terpene ozonolysis with two dicarboxylic acids

Yuanyuan Luo et al.

Correspondence to: Yuanyuan Luo (yuanyuan.luo@helsinki.fi) and Mikael Ehn (mikael.ehn@helsinki.fi)

This file contains:

Figures S1-S24
Table S1-S3
Text S1-S3

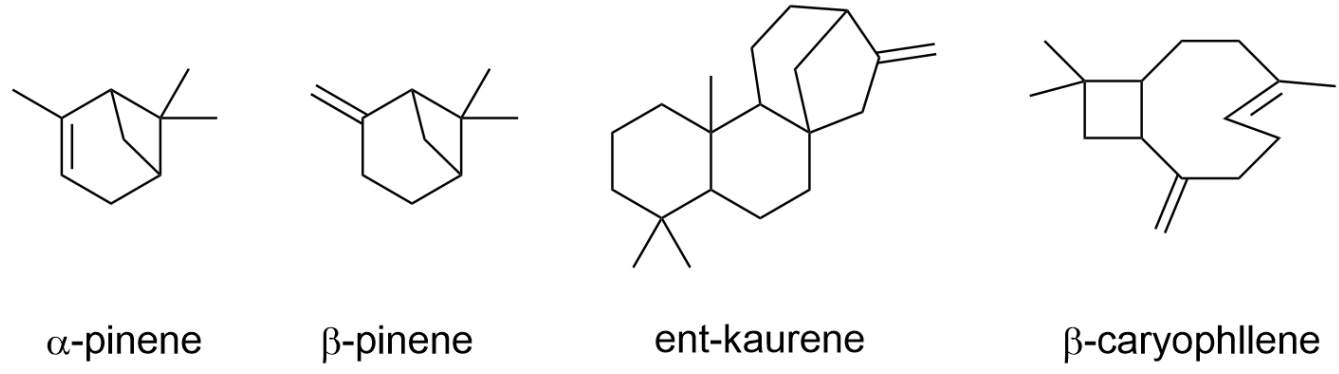

Figure S1. Structures of the terpenes.

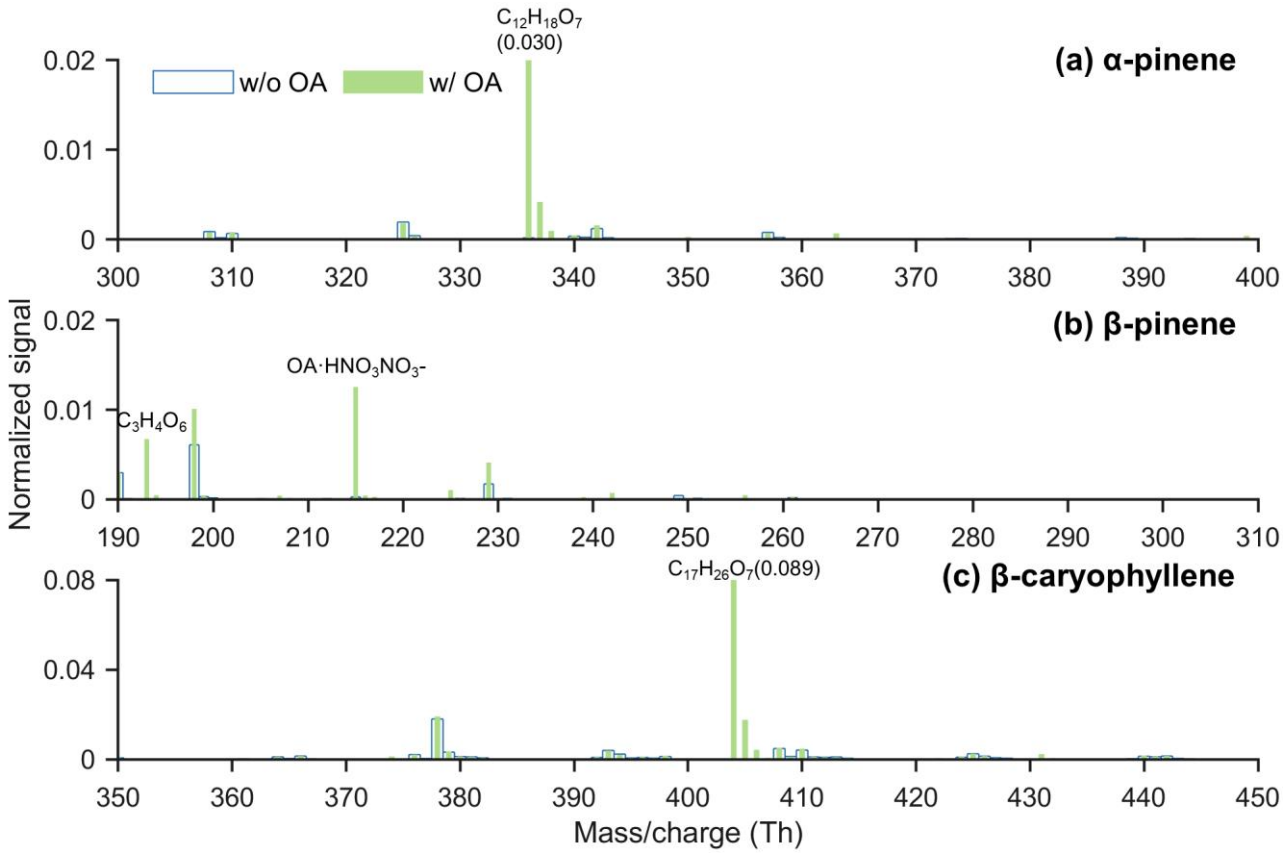

Figure S2. Mass spectrum of products formed from the ozonolysis of (a) α-pinene, (b) β-pinene, and (c) β-caryophyllene, both with and without the presence of oxalic acid.

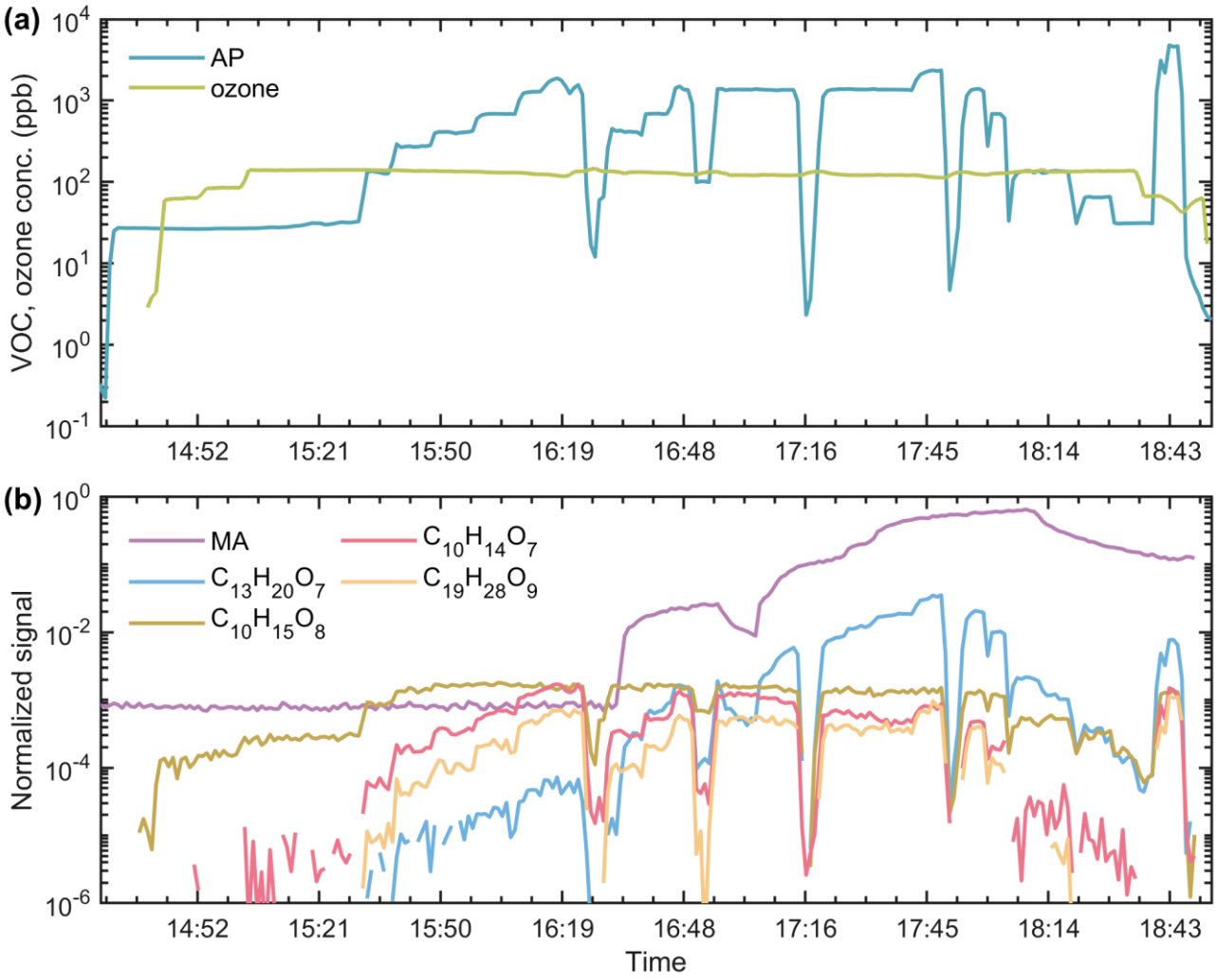

Figure S3. Time series of (a) α-pinene and ozone, (b) malonic acid, the dominant RO_2, HOM monomers, dimers, and accretion product of sCI + malonic acid.

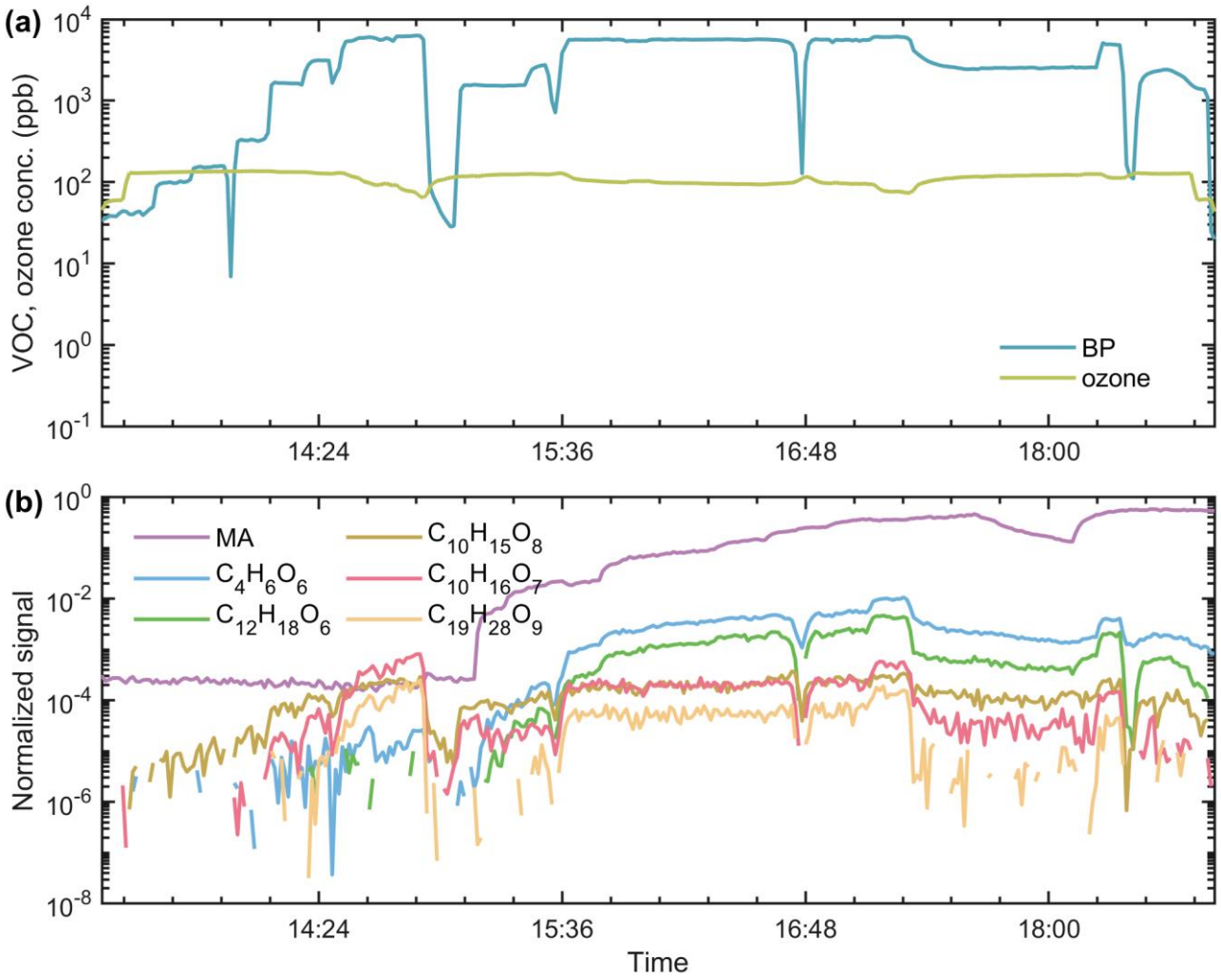

Figure S4. Time series of (a) β -pinene and ozone, (b) malonic acid, the dominant RO_2, HOM monomers, dimers, and accretion products of sCIs + malonic acid.

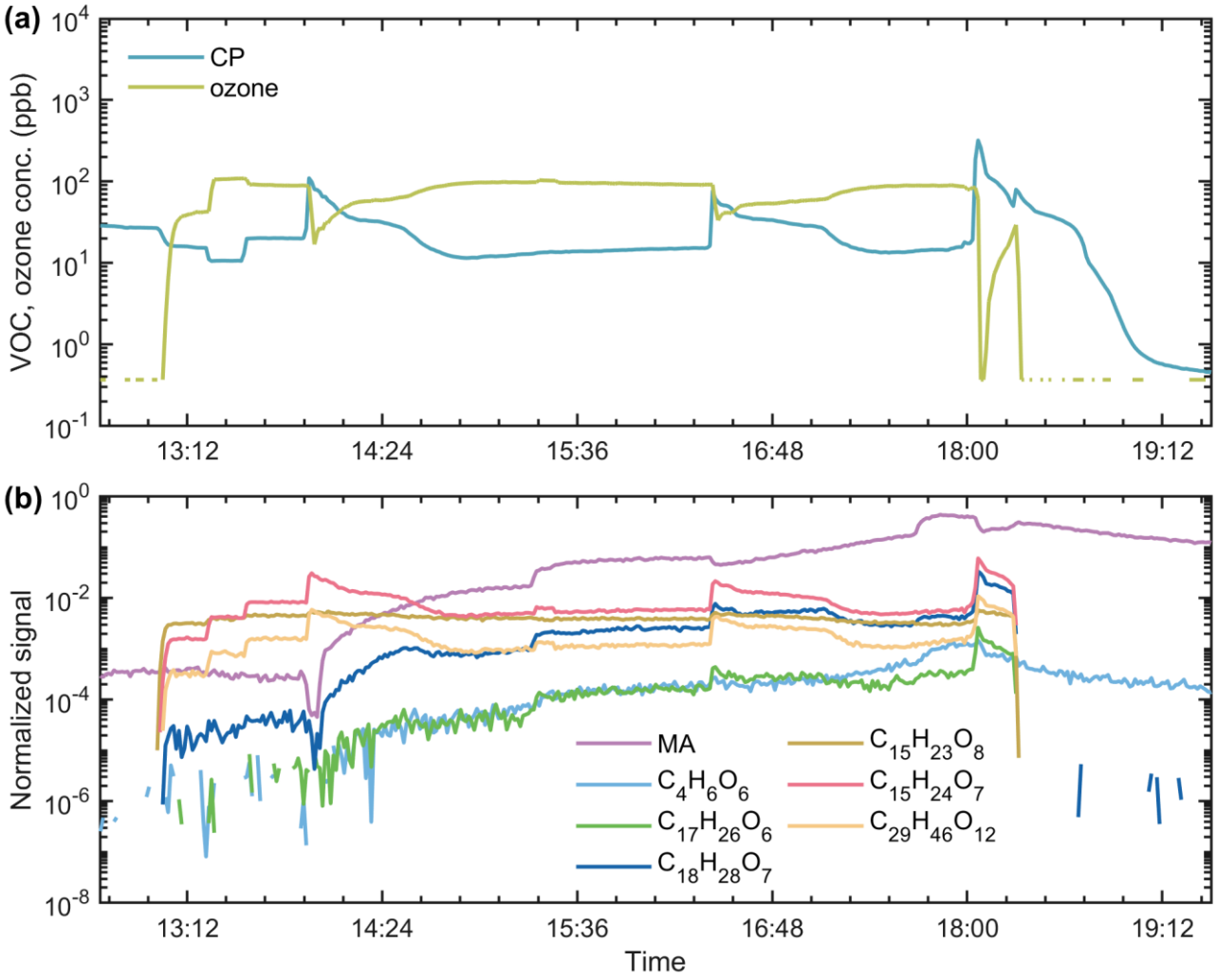

Figure S5. Time series of (a) β-caryophylle and ozone, (b) malonic acid, the dominant RO_2, HOM monomers, dimers, and accretion products of sCIs + malonic acid.

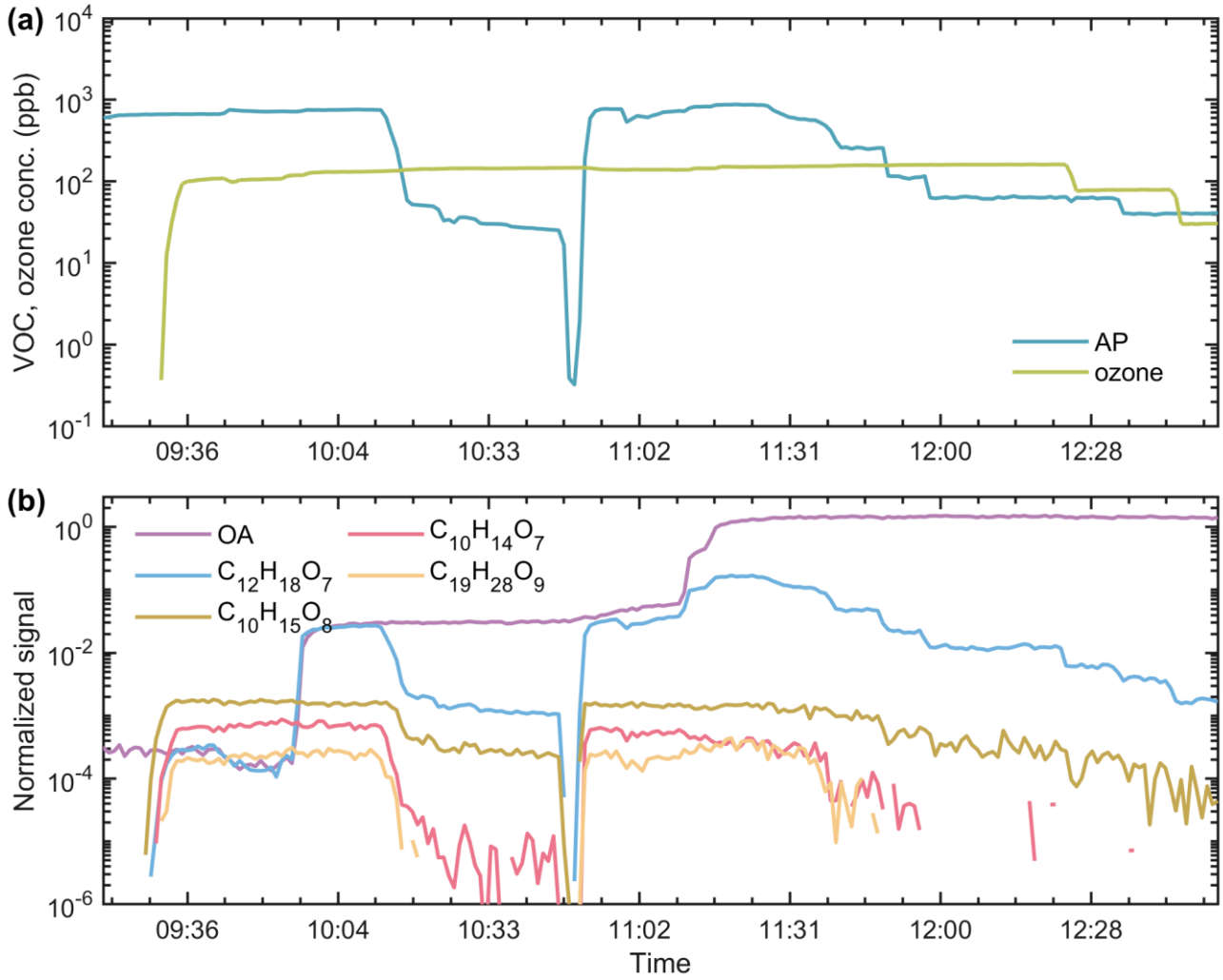

Figure S6. Time series of (a) α-pinene and ozone, (b) oxalic acid, the dominant RO_2, HOM monomers, dimers, and accretion product of sCI + oxalic acid.

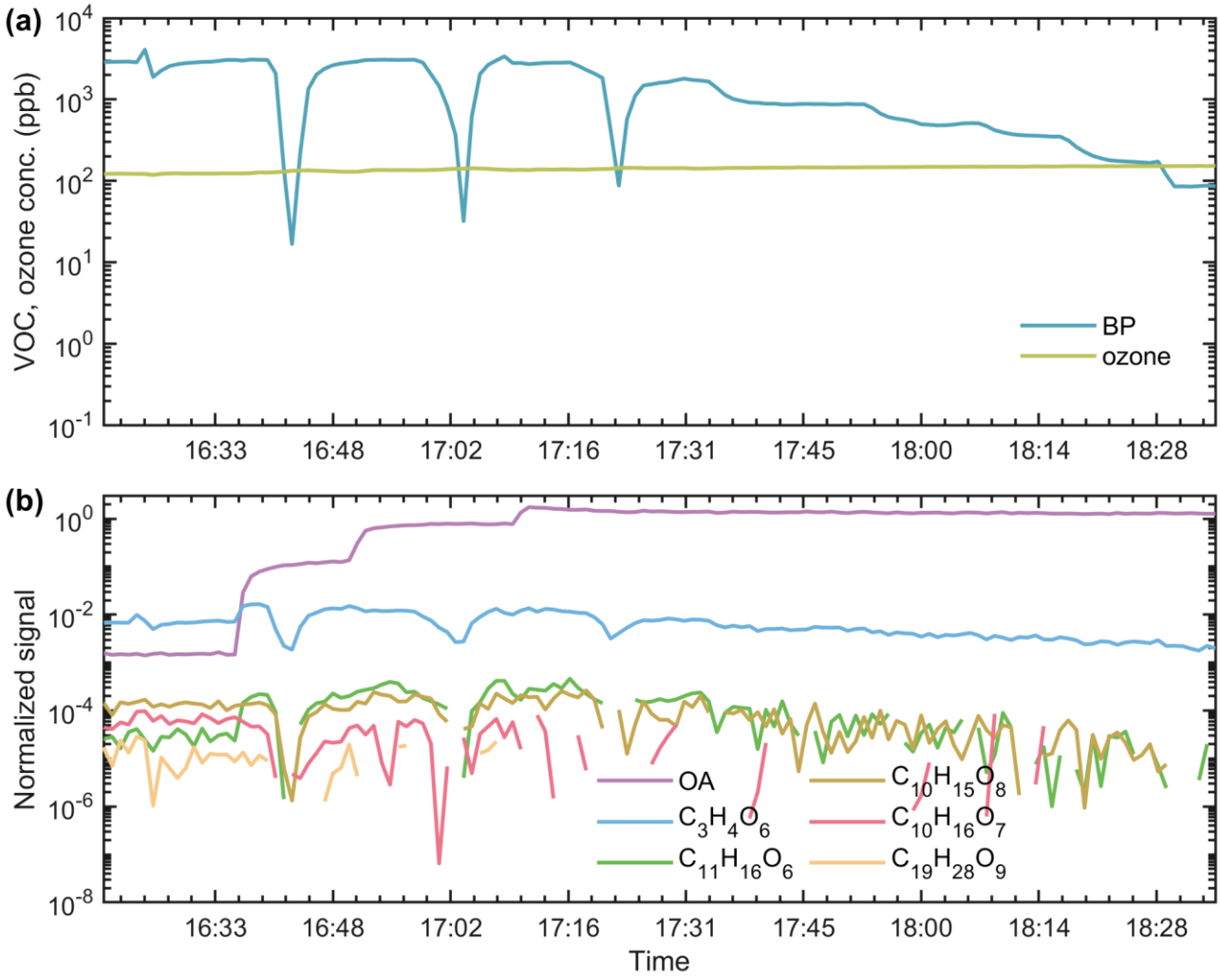

Figure S7. Time series of (a) β-pinene and ozone, (b) oxalic acid, the dominant RO_2, HOM monomers, dimers, and accretion products of sCIs + oxalic acid.

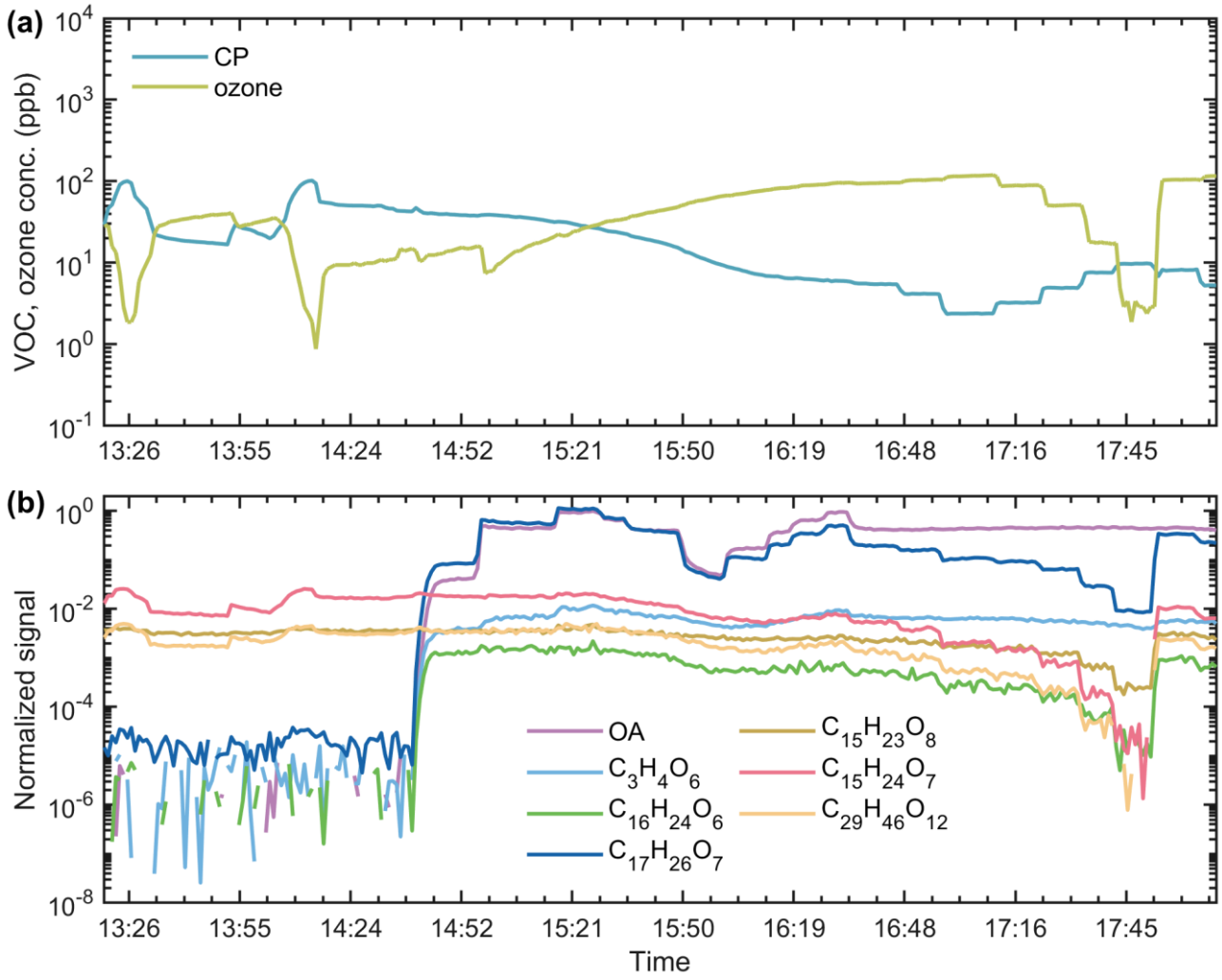

Figure S8. Time series of (a) β-caryophylle and ozone, (b) oxalic acid, the dominant RO_2, HOM monomers, dimers, and accretion products of sCIs + oxalic acid.

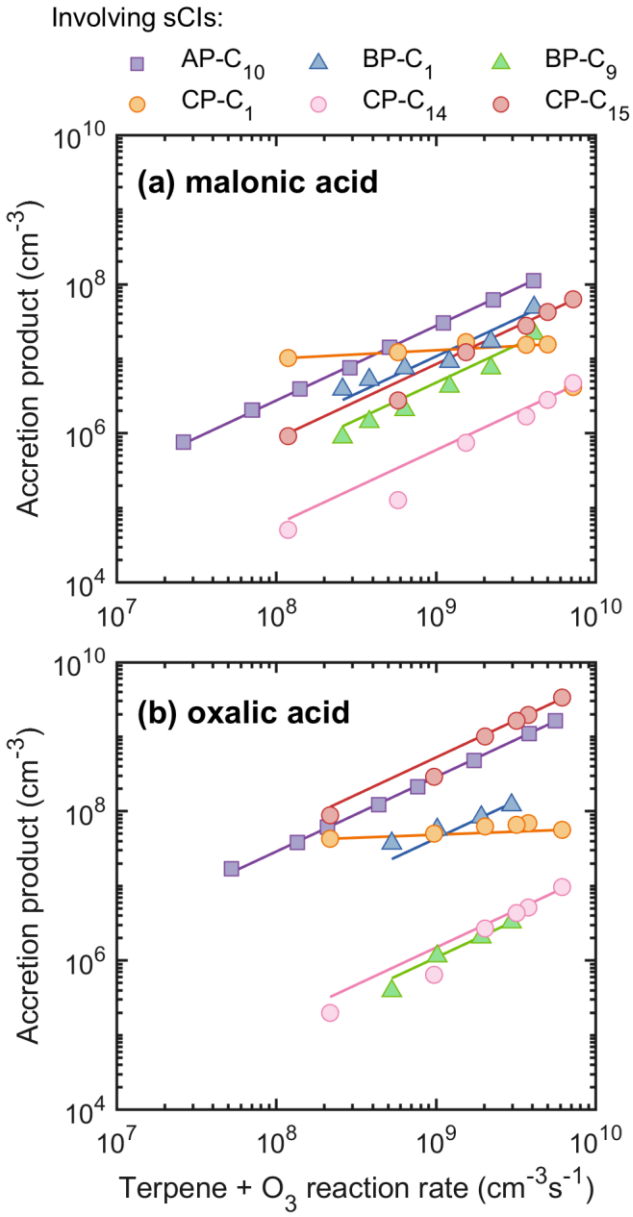

Figure S9. Concentrations of accretion products from sCIs with (a) malonic acid and (b) oxalic acid plotted against the ozonolysis rate of terpenes. The lines represent linear fits. Legend labels indicate different accretion products formed from various sCIs in reaction with the acids. For instance, AP-C_{10} in panel (a) corresponds to the accretion product $C_{13}H_{20}O_7$, formed from the sCI $C_{10}H_{16}O_3$ with malonic acid; similarly, AP-C_{10} in panel (b) corresponds to the accretion product $C_{12}H_{18}O_7$, formed from the same sCI reacting with oxalic acid.

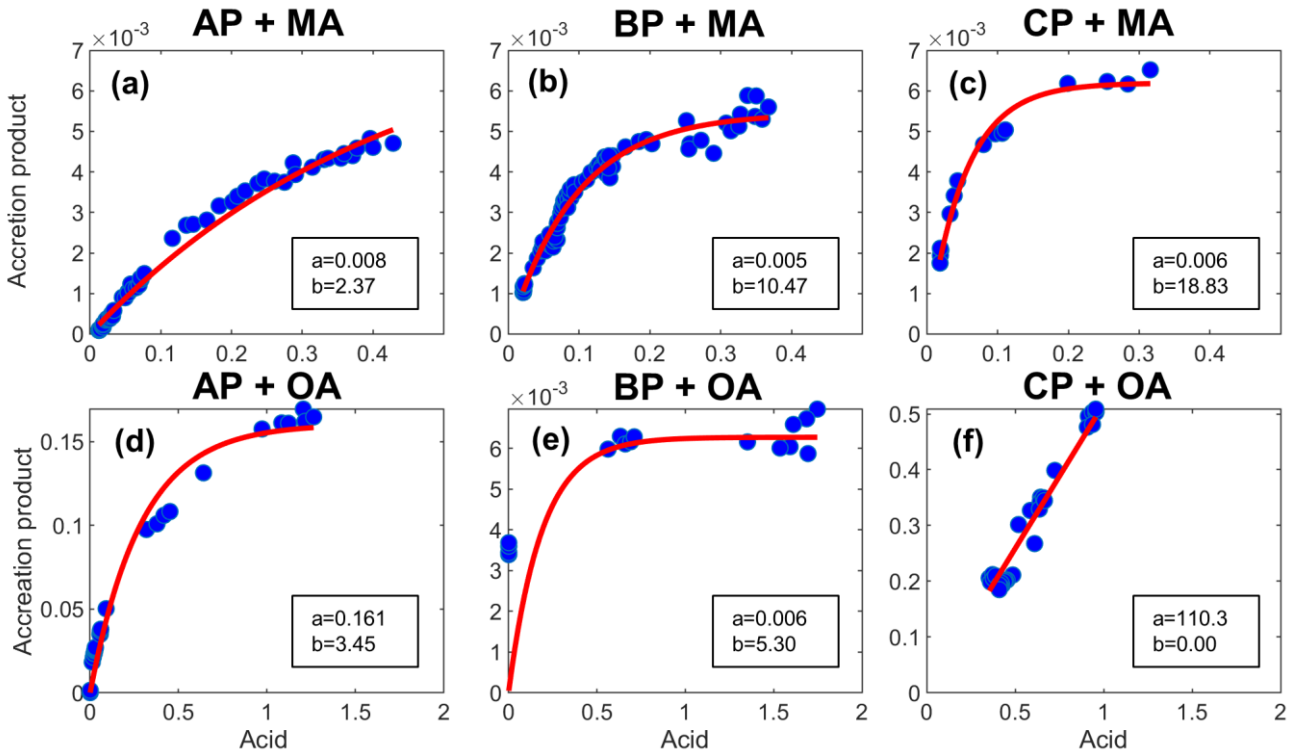

Figure S10. Normalized signal of the predominant accretion product of acid + sCI originating from the ozonolysis of α-pinene (AP), β-pinene (BP), and β-caryophyllene (CP) as a function of acid concentration. The red lines represent the fitted function applied to the observed data, using the expression: y = a * (1 - exp(-b * x)).

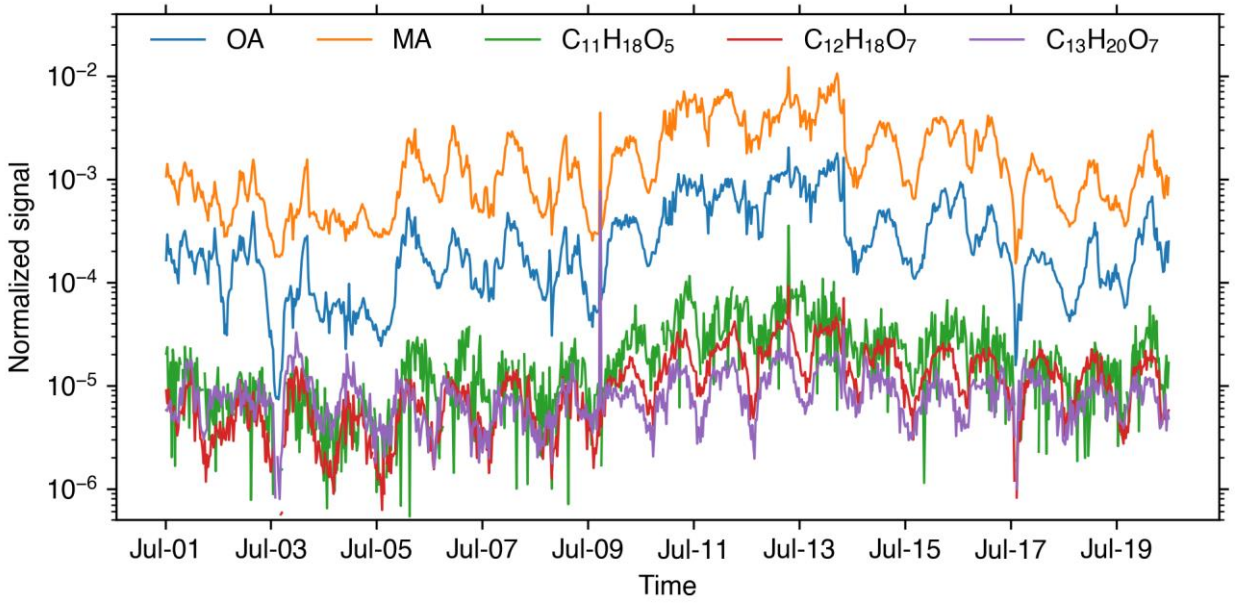

Figure S11. Time series of malonic acid, oxalic acid and three potential accretion products from α-pinene-derived sCIs and organic acids adducting in Hyytiälä during July 2023.

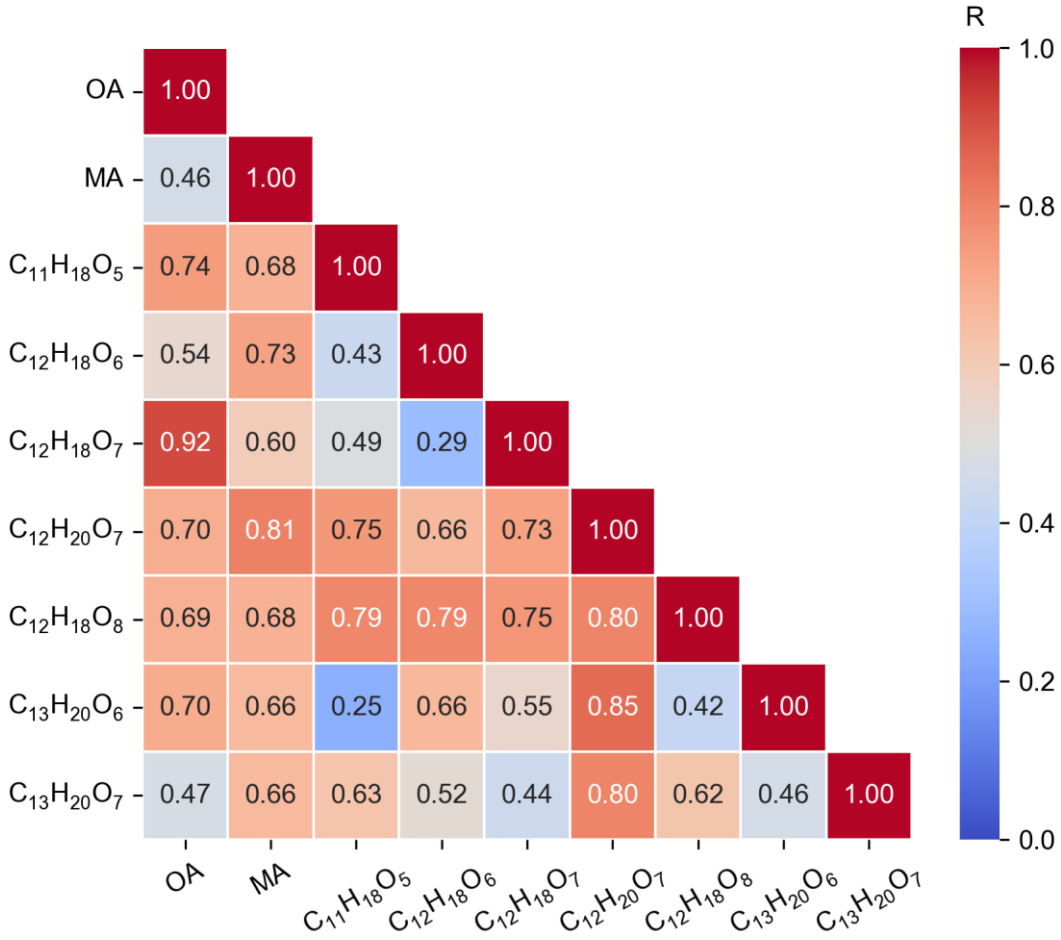

Figure S12. Correlation among malonic and oxalic acids and observed C_{12} and C_{13} species with decent signal intensities during the whole growing seasons (May – August 2023).

Text S1: Confirmation of the barrierlessness of the sCI + dicarboxylic acid reaction

According to Vereecken, the sCI may attack the carboxylic acid either through a 1,4-insertion into the O=C–OH moiety or through a 1,2-insertion into the OH bond (Vereecken, 2017). The first of these reaction channels is fully barrierless, and the second proceeds through a transition state submerged in energy relative to the separated products. Both reaction channels result in the same product, an α-acyloxy hydroperoxide. Vereecken determined the rate coefficients of these reactions using microvariational transition state theory due to the majority of the reaction proceeding through the barrierless channel. We decided not to perform calculations of this caliber for our C_9 and C_{10} sCIs, as this this would come with a high computational cost. Instead, we simply optimized the 1,2-insertion transition state for CH_2OO + Oxalic Acid and CH_2OO + Malonic Acid to test if these are similarly submerged in energy relative to the isolated reactants. Geometry optimization and frequency analysis

were performed using wB97X-D3/jun-cc-pV(T+d)Z, on top of which a single-point energy correction was performed with DLPNO-CCSD(T)/aug-cc-pVTZ with aug-cc-pVQZ auxillery basis. The calculations were performed with ORCA version 5.0.4. The resulting zero-point corrected energies of the transition states relative to the isolated reactants and products are shown in Table S1, and a visualisation of the transition states is shown in Figure S13. The results show that the 1,2-insertion transition states are even more submerged in energy for Oxalic and Malonic acid than for formic acid, indicating that these two sCI + Dicarboxylic reaction rate are unrestricted by energy. We assume this is the case also for the other sCI + Dicarboxylic acid reactions discussed in this work.

Table S1. Relative energies of the sCI + acid 1,2-insertion transition states and accretion products.

[a] From Vereecken (2017).

Ee + EZPE (kJ/mol)	CH2OO + Formic acid	CH2OO + Oxalic acid	CH2OO + Malonic acid
Reactants	0.00	0.00	0.00
Transition State	-10	-14.02	-25.33
Product	-186	-179.36	-203.30

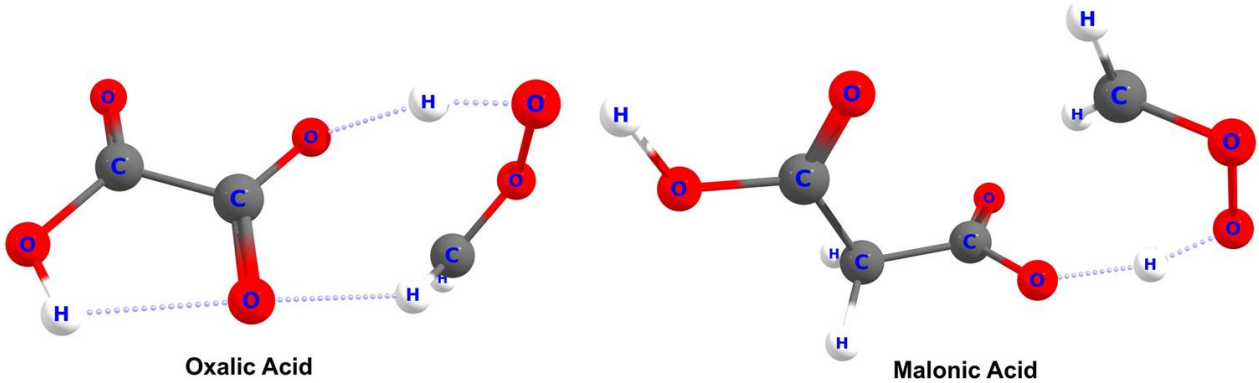

Figure S13. Transition state geometries for the 1,2-insertion of sCI into the dicarboxylic acids.

Text S2: Estimation of reaction rate coefficients

As shown above, we may assume that the sCI + Dicarboxylic acids are energetically barrierless, which means they are largely driven by long-range dipole-dipole interactions. Thus, the reaction rate coefficients of sCI + Malonic Acid were estimated using the Structure-Activity Relationship by Chhantyal-Pun et al. (2018) (Equation S1), with the conformer-averaged molecular dipole moment for Malonic Acid calculated using B3LYP/aug-cc-pVTZ (Lee et al., 1988; Kendall et al., 1992). For the BP-C_9 and AP-C_{10} isomers we used the corresponding values provided by Chhantyal-Pun et al. (2018) The reaction rate coefficients predicted using these are shown in Table S2. However, we were not able to use the same SAR for the sCI + Oxalic

Acid reactions, due to oxalic acid having a dipole moment of zero in its most likely conformer. Thus we estimated these rate coefficients using collision theory (Equation S2), with the collision surface of the molecules calculated assuming a scaled van der Waals surface (Lange and Herbert, 2010). These surface calculations were performed for the B3LYP/aug-cc-pVTZ - optimized molecular geometries using the CPCM module in ORCA (Garcia-Ratés and Neese, 2020). The results of these calculations are shown in Table S2. Despite both Malonic acid and Oxalic acid being dicarboxylic acids, the reaction rate coefficients were not multiplied by a reaction path degeneracy factor of 2, as the used models already assume that all molecular collisions lead to a reaction.

$$k_{Mal} = \frac{1}{\sqrt{\mu}}\left((d_{sCI}d_{Mal})^{2/3}1.9 \cdot 10^{-21} - 6.3 \cdot 10^{-21}\right)cm^3s^{-1} \quad S1$$

$$k_{Oxa} = \sqrt{\frac{8kT}{\pi\mu}}\left(\sigma_{sCI} + \sigma_{Oxa} + 2\sqrt{\sigma_{sCI}\sigma_{Oxa}}\right) \quad S2$$

In the equations, μ is the reduced mass of the two-particle system composed of the sCI and the acid, d_X is the dipole moment of molecule X, k is the Boltzmann constant, T is the temperature and σ_X is the collision surface of molecule X.

Table S2. Estimated reaction rate coefficients for the α-pinene and β-pinene derived Criegee intermediates with the dicarboxylic acids, along with the parameters these were calculated with.

	Dipole moment (D)	sCI + MA ($cm^3\ s^{-1}$)	vdW Surface ($Bohr^2$)	sCI + OA ($cm^3\ s^{-1}$)
Malonic acid	3.82			
Oxalic acid	40.02		399.3734	
CH2OO	4.31	8.24E-10	280.9004	2.20E-10
AP-syn-Pinonaldehyde o.	5.11	7.11E-10	854.345	2.79E-10
AP-anti-Pinonaldehyde o.	5.45	7.69E-10	880.8175	2.85E-10
AP-syn-Isopinonaldehyde o.	4.56	6.16E-10	878.891	2.84E-10
AP-anti-Isopinonaldehyde o.	4.80	6.58E-10	866.7562	2.82E-10
BP-syn-Nopinone o.	6.30	9.39E-10	708.7197	2.59E-10
BP-anti-Nopinone o.	6.45	9.64E-10	708.4969	2.58E-10

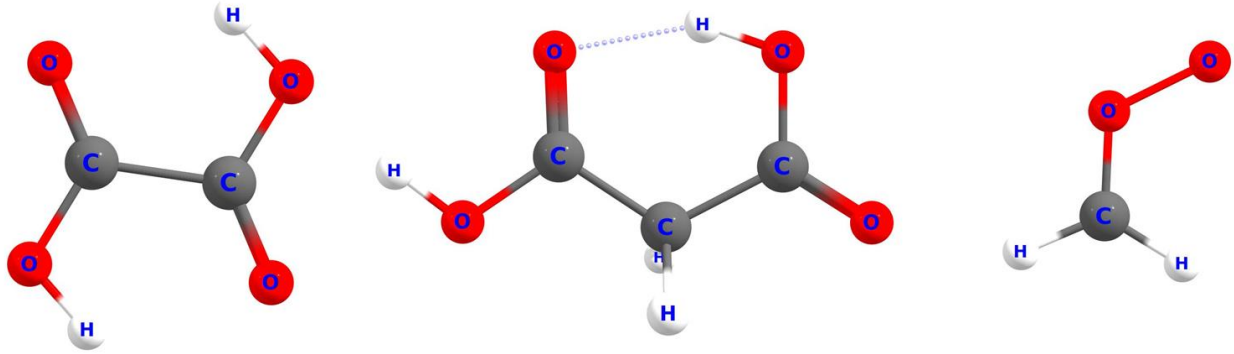

Figure S14. Lowest free energy conformers of Oxalic acid (left), Malonic acid, and CH_2OO (right)

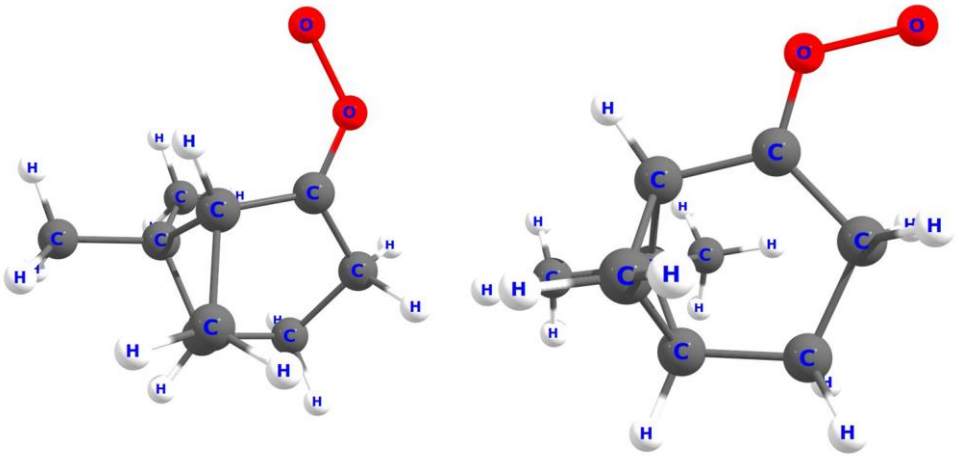

Figure S15. Syn-nopinone oxide (left) and anti-nopinone oxide (right).

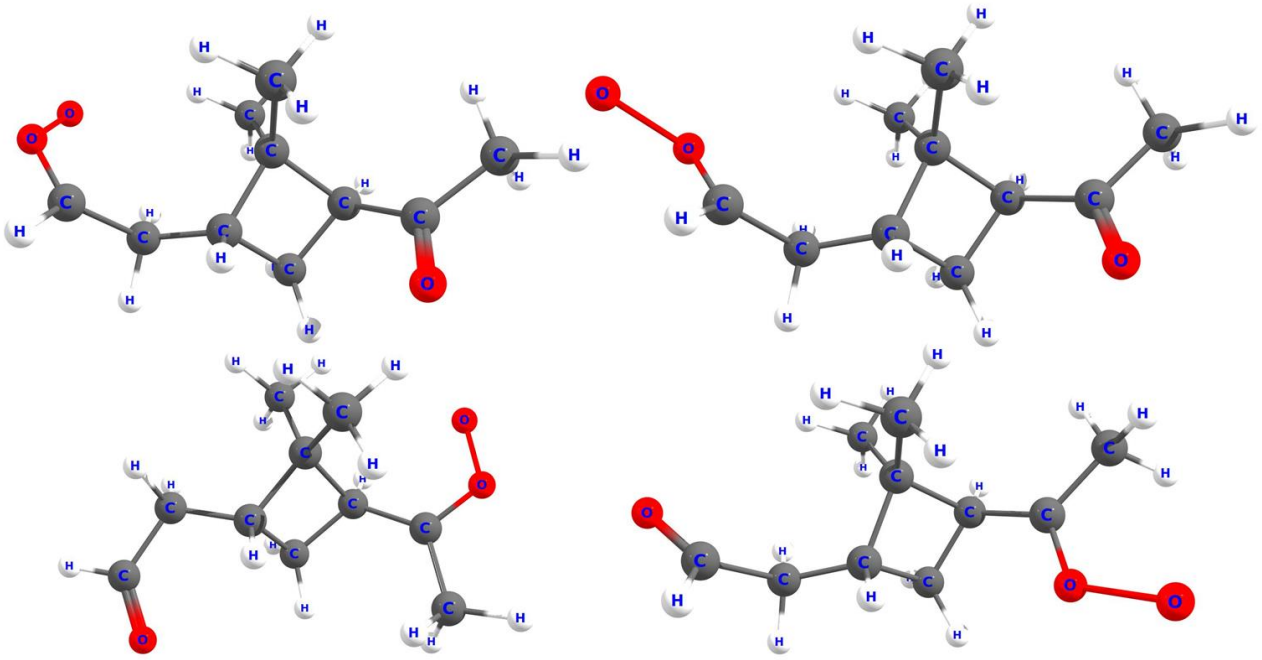

Figure S16. Lowest free energy conformers of syn-pinonaldehyde oxide (top left), anti-pinonaldehyde oxide (top right), syn-isopinonaldehyde oxide (bottom left), and anti-isopinonaldehyde oxide (bottom right).

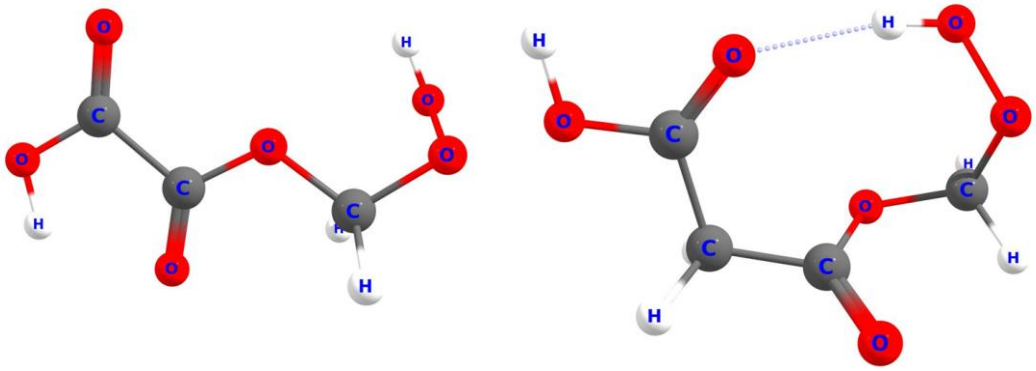

Figure S17. Lowest free energy conformers of CH_2OO accretion products with Oxalic acid (left) and malonic acid (right).

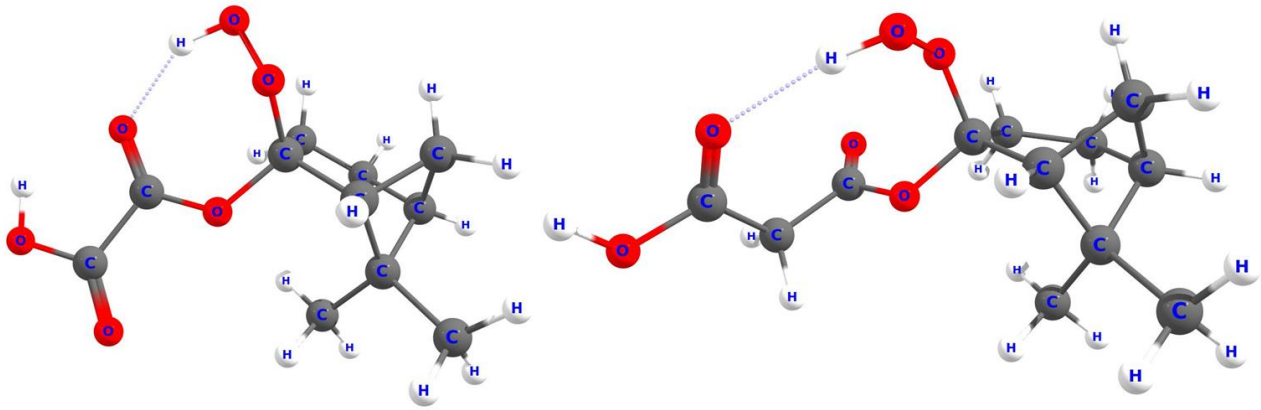

Figure S18. Lowest free energy conformers of Nopinene oxide accretion products with oxalic acid (left) and malonic acid (right).

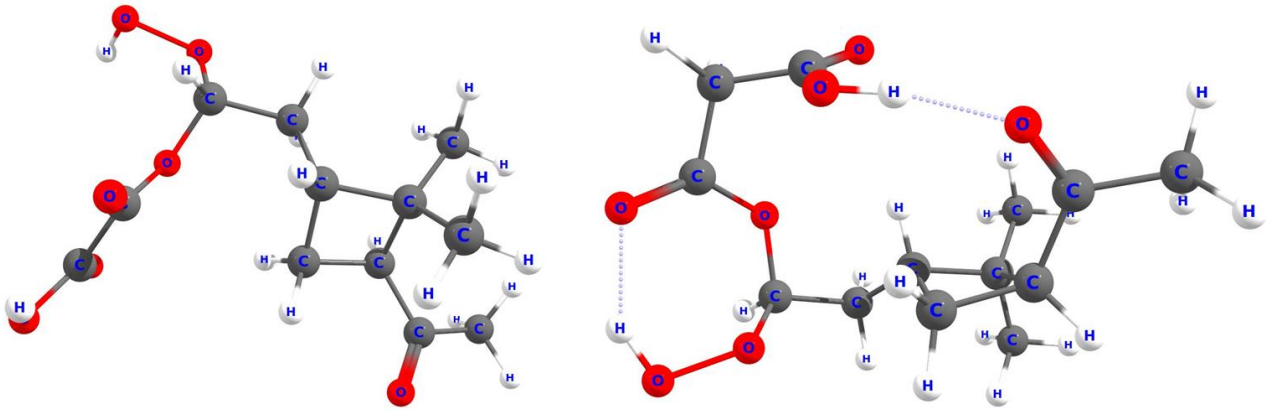

Figure S19. Lowest free energy conformers of pinonaldehyde oxide accretion products with oxalic acid (left) and malonic acid (right).

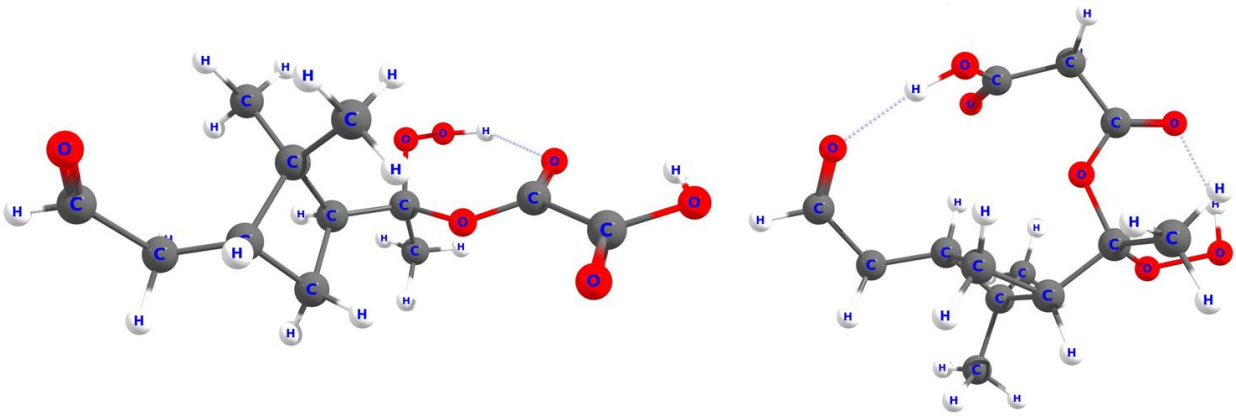

Figure S20. Lowest free energy conformers of isopinonaldehyde oxide accretion products with oxalic acid (left) and malonic acid (right).

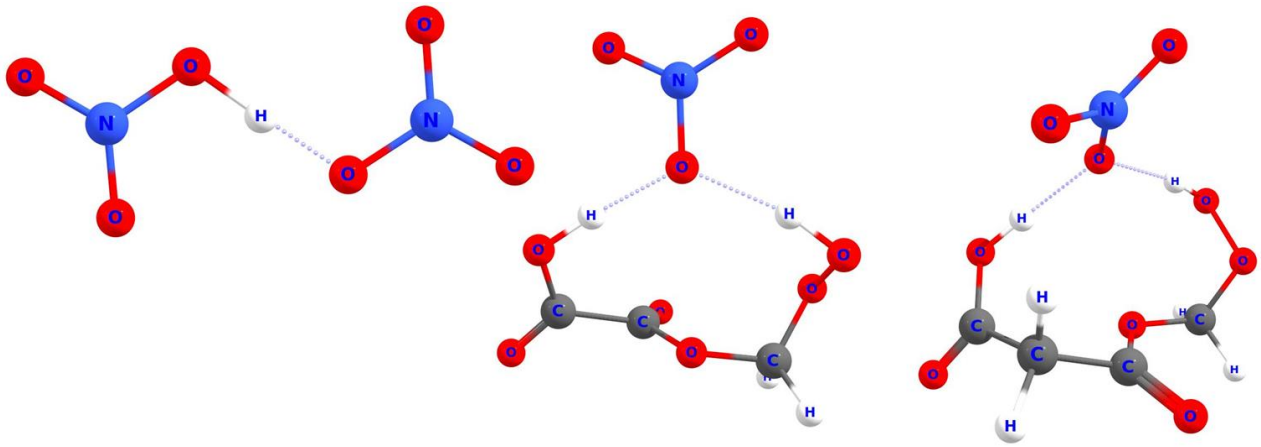

Figure S21. Lowest free energy conformers of the nitrate ion clusters of nitric acid and the CH_2OO accretion products with oxalic acid (centre) and malonic acid (right).

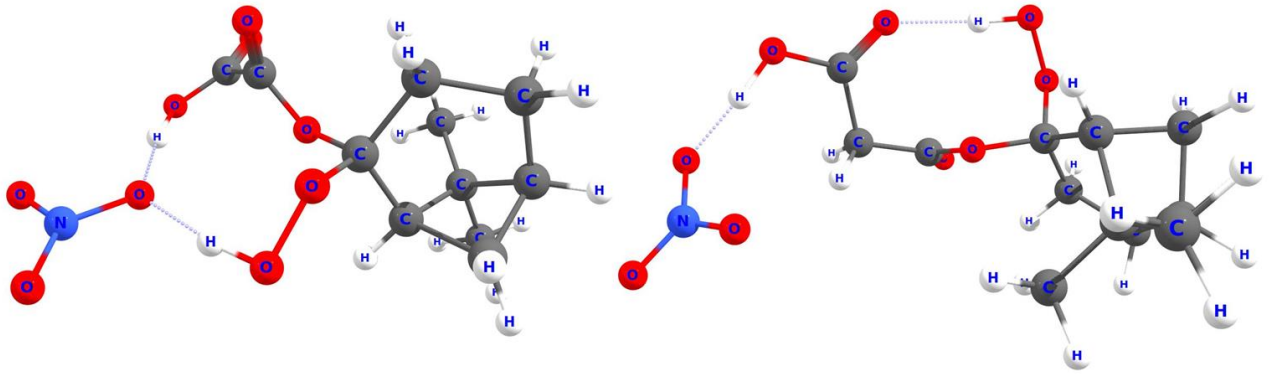

Figure S22. Lowest free energy conformers of the nitrate ion clusters of Nopinone oxide with oxalic acid (left) and malonic acid (right).

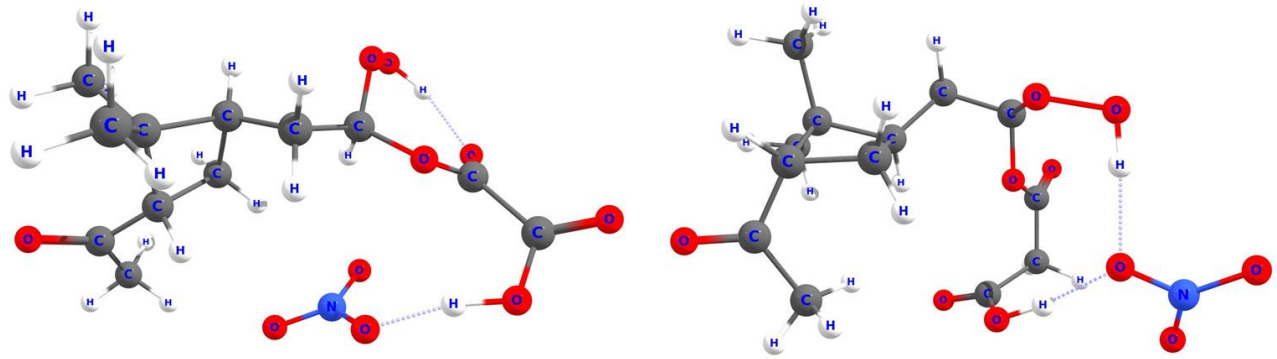

Figure S23. Lowest free energy conformers of the nitrate ion clusters of Pinonaldehyde oxide with oxalic acid (left) and malonic acid (right).

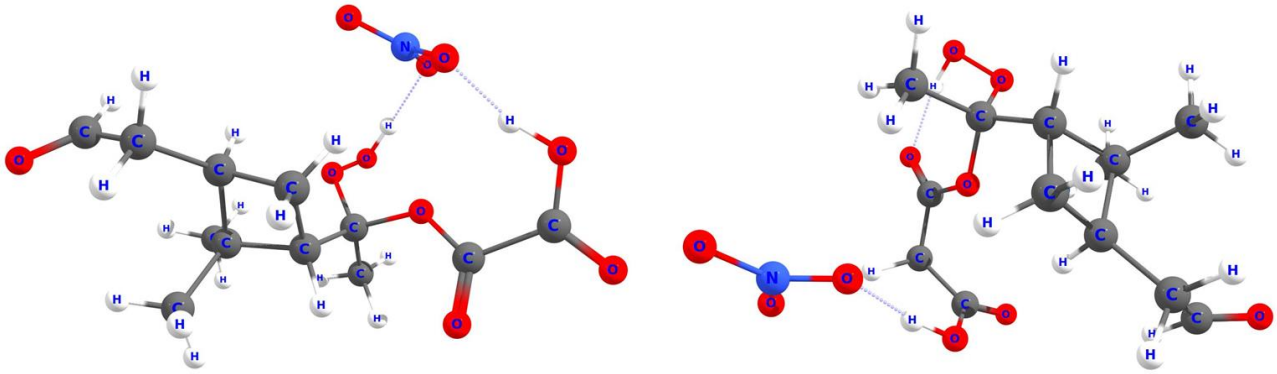

Figure S24. Lowest free energy conformers of the nitrate ion clusters of Isopinonaldehyde oxide with oxalic acid (left) and malonic acid (right).

Text S3: NO_3-CIMS detection sensitivities of accretion products

The Gibbs free energies of clustering are calculated using equation S3, where the subscript Acc refers to the accretion product and clust refers to the NO_3^- ion cluster of the same product. E is the energy, which is a sum of electronic, vibrational zero-point, and thermal contributions, whereas S_X is the entropy of system X. The electronic energy component is received from the result of the DLPNO-CCSD(T) calculations, whereas the rest (lumped in the ORCA output as G - E(el)) are received from the ωB97X-D3 calculations. The results of the clustering calculations are presented in Table S3.

$$\Delta G = E_{clust} - E_{NO3} - E_{Acc} - kT + T(S_{NO3} + S_{Acc} - S_{clust}) \quad S3$$

$$E = E_e + E_{ZPE} + E_T(T) \quad S4$$

The Gibbs free energy of clustering with the NO_3^- ion for the α-pinene and β-pinene derived accretion products were calculated similarly as in Hyttinen et al. (2015) with the following scheme used for conformer sampling and filtering: The initial set of conformers for each accretion product and cluster was generated using metadynamics with the XTB-GFN2 level of theory (Bannwarth et al., 2019) using the CREST software (Pracht et al., 2024). For each generated conformer a single-point energy calculation was performed using B3LYP/6-31+G*, after which the conformers were filtered for uniqueness using the electronic energy and dipole moment cutoffs from Møller et al. (2016). In the next step, all unique conformers with electronic energies within 21 kJ/mol of the minimum value were optimized with B3LYP/ma-def2-SVP (Zheng et al., 2011). After a second round of uniqueness filtering, all unique conformers with electronic energies within 9 kJ/mol of the minimum value were reoptimized with ωB97X-D3/jun-cc-pV(T+d)Z (Lin et al., 2013; Papajak et al., 2011), with analytical frequency calculations performed for each conformer. Finally, a single-point energy calculation using DLPNO-CCSD(T)/aug-cc-pVTZ with aug-cc-pVQZ auxillery basis (Saitow et al., 2017; Riplinger et al., 2013; Riplinger et al., 2016; Riplinger and Neese, 2013; Neese et al., 2009b; Neese et al., 2009a; Bistoni et al., 2017) was calculated for the conformer with the lowest Gibbs free energy. The final DLPNO-CCSD(T) calculation proved too costly for the NO_3^- clusters of the α-pinene-sCI + malonic acid accretion products, so the jun-cc-pV(T+d)Z basis set with cc-pVQZ auxillery basis was used instead.

Table S3. Gibbs free energies of clustering at temperature 298 K for the α-pinene and β-pinene derived accretion products, as well as for the nitric acid cluster for reference.

[a] From Hyttinen et al, calculated with DLPNO-CCSD(T)/def2-QZVPP single point on top of ωB97XD/aug-cc-pVTZ optimization.(Hyttinen et al., 2015)

[b] From Hyttinen et al. (2015), same methods as above (Hyttinen et al., 2017).

	ΔG (kJ/mol)	ΔE_e (kJ/mol)	ΔE_{ZPE} (kJ/mol)	-T ΔS (kJ/mol)
$(HNO_3)NO_3$[a]	-84.10	-121.34		
$(HNO_3)NO_3$[b]	-89.79	-122.47		
$(HNO_3)NO_3$	-81.95	-122.42	-3.00	43.47
CH_2OO-OA	-105.69	-159.71	3.86	50.16
BP-Nopinone-OA	-99.05	-150.10	2.97	48.08
AP-Pinonaldehyde-OA	-112.53	-172.03	4.34	55.16
AP-Isopinonaldehyde-OA	-102.10	-151.20	2.17	51.62
CH_2OO-MA	-93.54	-149.84	5.38	50.93
BP-Nopinone-MA	-95.60	-142.55	1.23	45.72
AP-Pinonaldehyde-MA	-97.70	-147.11	2.39	47.02
AP-Isopinonaldehyde-MA	-86.63	-134.50	1.52	47.43

In order for the accretion product to be detected efficiently in the CIMS experiments, the free energy of clustering of the accretion product must be lower than that of HNO_3, as the nitric acid solution from which NO_3^- ions are generated also produces large quantities of gas-phase HNO_3 in the inlet. Unfortunately, the exact binding free energy of this nitric acid complex is uncertain, as the shifting of the H atom between the two NO_3^- ions causes the potential well to have a double-well shape badly described by our typical frequency analysis methods. As seen in the comparison of the three ΔG and ΔE_e values in Table S3, the bulk of the uncertainty comes from the ZPE and S contributions for this system. We thus assume that the true ΔG value for $(HNO_3)NO_3$ may be anything between -80 and -90 kJ/mol.

Compared to the scale of reference values for $(HNO_3)NO_3$, we see that most of the considered accretion products cluster efficiently with the NO_3 radical, with the exception of the AP-Isopinonaldehyde-Mal, and possibly CH_2OO-Mal.

References

Bannwarth, C., Ehlert, S., and Grimme, S.: GFN2-xTB—An Accurate and Broadly Parametrized Self-Consistent Tight-Binding Quantum Chemical Method with Multipole Electrostatics and Density-Dependent Dispersion Contributions, Journal of Chemical Theory and Computation, 15, 1652-1671, 10.1021/acs.jctc.8b01176, 2019.

Bistoni, G., Riplinger, C., Minenkov, Y., Cavallo, L., Auer, A. A., and Neese, F.: Treating subvalence correlation effects in domain based pair natural orbital coupled cluster calculations: an out-of-the-box approach, Journal of Chemical Theory and Computation, 13, 3220-3227, 2017.

Chhantyal-Pun, R., Rotavera, B., McGillen, M. R., Khan, M. A. H., Eskola, A. J., Caravan, R. L., Blacker, L., Tew, D. P., Osborn, D. L., Percival, C. J., Taatjes, C. A., Shallcross, D. E., and Orr-Ewing, A. J.: Criegee Intermediate Reactions with Carboxylic Acids: A Potential Source of Secondary Organic Aerosol in the Atmosphere, ACS Earth and Space Chemistry, 2, 833-842, 10.1021/acsearthspacechem.8b00069, 2018.

Garcia-Ratés, M. and Neese, F.: Effect of the Solute Cavity on the Solvation Energy and its Derivatives within the Framework of the Gaussian Charge Scheme, Journal of Computational Chemistry, 41, 922-939, 2020.

Hyttinen, N., Rissanen, M. P., and Kurtén, T.: Computational Comparison of Acetate and Nitrate Chemical Ionization of Highly Oxidized Cyclohexene Ozonolysis Intermediates and Products, The Journal of Physical Chemistry A, 121, 2172-2179, 10.1021/acs.jpca.6b12654, 2017.

Hyttinen, N., Kupiainen-Määttä, O., Rissanen, M. P., Muuronen, M., Ehn, M., and Kurtén, T.: Modeling the Charging of Highly Oxidized Cyclohexene Ozonolysis Products Using Nitrate-Based Chemical Ionization, The Journal of Physical Chemistry A, 119, 6339-6345, https://doi.org/10.1021/acs.jpca.5b01818, 2015.

Kendall, R. A., Dunning, T. H., and Harrison, R. J.: Electron affinities of the first-row atoms revisited. Systematic basis sets and wave functions, The Journal of chemical physics, 96, 6796-6806, 1992.

Lange, A. W. and Herbert, J. M.: A smooth, nonsingular, and faithful discretization scheme for polarizable continuum models: The switching/Gaussian approach, The Journal of chemical physics, 133, 2010.

Lee, C., Yang, W., and Parr, R. G.: Development of the Colle-Salvetti correlation-energy formula into a functional of the electron density, Physical review B, 37, 785, 1988.

Lin, Y.-S., Li, G.-D., Mao, S.-P., and Chai, J.-D.: Long-Range Corrected Hybrid Density Functionals with Improved Dispersion Corrections, Journal of Chemical Theory and Computation, 9, 263-272, 10.1021/ct300715s, 2013.

Møller, K. H., Otkjær, R. V., Hyttinen, N., Kurtén, T., and Kjaergaard, H. G.: Cost-Effective Implementation of Multiconformer Transition State Theory for Peroxy Radical Hydrogen Shift Reactions, The Journal of Physical Chemistry A, 120, 10072-10087, 10.1021/acs.jpca.6b09370, 2016.

Neese, F., Hansen, A., and Liakos, D. G.: Efficient and accurate approximations to the local coupled cluster singles doubles method using a truncated pair natural orbital basis, The Journal of chemical physics, 131, 2009a.

Neese, F., Wennmohs, F., and Hansen, A.: Efficient and accurate local approximations to coupled-electron pair approaches: An attempt to revive the pair natural orbital method, The Journal of chemical physics, 130, 2009b.

Papajak, E., Zheng, J., Xu, X., Leverentz, H. R., and Truhlar, D. G.: Perspectives on Basis Sets Beautiful: Seasonal Plantings of Diffuse Basis Functions, Journal of Chemical Theory and Computation, 7, 3027-3034, 10.1021/ct200106a, 2011.

Pracht, P., Grimme, S., Bannwarth, C., Bohle, F., Ehlert, S., Feldmann, G., Gorges, J., Müller, M., Neudecker, T., and Plett, C.: CREST—A program for the exploration of low-energy molecular chemical space, The Journal of Chemical Physics, 160, 2024.

Riplinger, C. and Neese, F.: An efficient and near linear scaling pair natural orbital based local coupled cluster method, The Journal of chemical physics, 138, 2013.

Riplinger, C., Sandhoefer, B., Hansen, A., and Neese, F.: Natural triple excitations in local coupled cluster calculations with pair natural orbitals, The Journal of chemical physics, 139, 2013.

Riplinger, C., Pinski, P., Becker, U., Valeev, E. F., and Neese, F.: Sparse maps—A systematic infrastructure for reduced-scaling electronic structure methods. II. Linear scaling domain based pair natural orbital coupled cluster theory, The Journal of chemical physics, 144, 2016.

Saitow, M., Becker, U., Riplinger, C., Valeev, E. F., and Neese, F.: A new near-linear scaling, efficient and accurate, open-shell domain-based local pair natural orbital coupled cluster singles and doubles theory, The Journal of chemical physics, 146, 2017.

Vereecken, L.: The reaction of Criegee intermediates with acids and enols, Physical Chemistry Chemical Physics, 19, 28630-28640, 2017.

Zheng, J., Xu, X., and Truhlar, D. G.: Minimally augmented Karlsruhe basis sets, Theoretical Chemistry Accounts, 128, 295-305, 10.1007/s00214-010-0846-z, 2011.